Dynamics of metamaterial beams consisting of periodically-coupled parallel flexural elements: A theoretical study

Setare Hajarolasvadi and Ahmed E. Elbanna

Department of Civil and Environmental Engineering, University of Illinois, Urbana-Champaign, Illinois, USA

Abstract

Periodic systems have attracted a lot of attention in science and engineering due to the existence of band gaps in their frequency spectra. Here, we study the flexural wave propagation in beams that are periodically connected in parallel and investigate how the contrast in the material and cross-sectional properties may affect the band structure of these systems and their dispersion properties. Results suggest that by changing the mass and stiffness ratios of the two beams, or by changing the inter-beam connection compliance, several band gaps may emerge and that the band gap width, the lowest band gap edge frequency, as well as the nature of attenuation within the gap may be tuned. Furthermore, by considering a hierarchical system of periodically-connected beam elements with different unit cell sizes, we show how the interplay between scales may affect the overall dispersion properties of the system by opening and closing band gaps at different frequencies. These findings suggest that a modular design approach may lead to novel dispersion properties in beam structures. Finally, using a Frequency Response Function approach, we show that the aforementioned results hold in the limit of finite structures.

1 Introduction

Wave propagation in periodic structures has been investigated for decades: from large-scale structures, such as multi-story buildings, multi-span bridges and pipelines [1–4] to atomic lattices [5]. These structures have been a focus of attention due to their wave-filtering properties. It has been well-established that waves in certain frequency ranges cannot freely propagate in periodic systems due to the existence of band gaps in their frequency spectra [6]. This feature has made them potential candidates for applications such as vibration and seismic isolation [7–9], wave-guiding [10–12] and cloaking [13–15]. Two mechanisms have been identified for band gap formation in periodic systems: Bragg scattering (BS) and local resonance (LR). Bragg band gaps occur due to multiple scattering and interference effects between the periodic constituents of the system. Hence, these gaps occur at wavelengths comparable to the structural periodicity. The seminal work of Liu et al. [16], however, showed that gaps can occur at frequencies nearly two orders of magnitude lower than that of the Bragg frequency if local resonance is exploited. In an attempt to further enhance the dispersion characteristics of these systems, researchers have recently proposed novel designs that aim to combine the features of both mechanisms. These designs range from systems with interconnected resonators [17, 18] to configurations with resonators directly attached to neighboring masses in the host structure [19].

Periodic beams have been particularly studied to a great extent in literature. As early as the 1960s, the natural frequencies and steady-state responses of beams with periodic supports and periodic impedances were studied [20, 21]. Since then, many researchers have investigated flexural vibration band gaps in beams with various periodicity features. Attention was first drawn to periodic beams with a binary configuration, in which the unit cell consists of two flexural elements with different

material or geometric properties placed in series [1, 22, 23]. The Bragg scattering mechanism is responsible for band gap formation in these structures. More recent studies have focused on Locally Resonant (LR) beams, in which a periodic array of local resonators leads to the emergence of band gaps in the frequency spectra of the system [24–29]. Band gaps in this class of structures form due to both BS and LR mechanisms [30, 31]. Liu and Hussein studied wave propagation in flexural beams from both categories and mathematically characterized the condition for transition between Bragg scattering and local resonance band gaps in LR beams [32]. Most research in the area of LR beams has focused mainly on the effect of discrete resonators. However, recently, Wang et al. studied a local resonant beam with continuum beam resonators and proved its effectiveness in comparison with the conventional force-only resonators [33]. Beli et al. proposed a metamaterial beam with interconnected beam attachments, forming a resonator chain. The authors showed that the interaction between the translational and rotational modes of this chain enriches the band structure in comparison to the case where the beam resonators perform independently[18].

Studying structures that are periodically connected in parallel could be traced back to Sen Gupta's work in 1970 on the so-called rib-skin structures [34], encountered in airplane applications. These structures consist of a pair of plates (skins) joined periodically in parallel by another set of orthogonal plates (ribs). The ribs are usually modeled as rigid bodies while the skins are modeled as elastic beams. Gupta showed that the dispersion relation of one such structure is quadratic in $\cosh \mu$, where μ is the propagation constant, and identified the propagation and attenuation zones. More work has been done since on stiffened plates and beams in the context of periodic systems [35–37]. More recently, Chen and Elbanna studied the coupling of a pair of bars in parallel and showed that tailoring the properties of the two elastic members may lead to extreme attenuation zones in the band structure of the system. The idea was then used to realize a mechanical switch that is used to modulate elastic waves [38].

In this paper, we focus our attention on parallel beam elements that are periodically connected by enforcing compatibility of deformation and force balance at discrete attachment points along their length. We carry out a parametric study to show the effects of material and section properties as well as connection compliance on the band structure of the system. We, then, show that the system may possess rich dispersion properties in the low frequency ranges by tuning the parameters properly.

2 Methods

2.1 Analytical model

Rigid connections The setup of the metamaterial beam with rigid connections is shown in Fig. 1a. The system consists of two uniform beams periodically coupled with rigid arms that enforce equal transverse displacement and rotation at the connection points between the two beam elements. The spacing of the periodic attachments is L. The dynamics of the infinite metamaterial beam is studied by deriving the governing equations for one of its unit cells (Fig. 1b) following the Euler-Bernoulli beam theory and assuming that the coupling of the two beams is exactly imposed at the boundaries of the unit cell. The governing equations are written as follows:

$$\frac{\partial^2}{\partial x^2}[E_1 I_1 \frac{\partial^2 Y_1(x,t)}{\partial x^2}] + \rho_1 A_1 \frac{\partial^2 Y_1(x,t)}{\partial t^2} = 0 \tag{1a}$$

$$\frac{\partial^2}{\partial x^2}[E_2 I_2 \frac{\partial^2 Y_2(x,t)}{\partial x^2}] + \rho_2 A_2 \frac{\partial^2 Y_2(x,t)}{\partial t^2} = 0 \tag{1b}$$

where, ρ and E refer to the density and Young's modulus of the beam material, respectively and A and I denote the cross-sectional area and moment of inertia of the members. The solution of the PDEs is written as $Y_1(x,t) = y_1(x)e^{i\omega t}$ and $Y_2(x,t) = y_2(x)e^{i\omega t}$, where $y_1(x)$ and $y_2(x)$ are of

the following general form:

$$y_1(x) = a_{11}\cos\frac{\sqrt{\omega}x}{\beta_1} + a_{12}\sin\frac{\sqrt{\omega}x}{\beta_1} + a_{13}\cosh\frac{\sqrt{\omega}x}{\beta_1} + a_{14}\sinh\frac{\sqrt{\omega}x}{\beta_1} \tag{2a}$$

$$y_2(x) = a_{21}\cos\frac{\sqrt{\omega}x}{\beta_2} + a_{22}\sin\frac{\sqrt{\omega}x}{\beta_2} + a_{23}\cosh\frac{\sqrt{\omega}x}{\beta_2} + a_{24}\sinh\frac{\sqrt{\omega}x}{\beta_2} \tag{2b}$$

Here, $\beta_j = \sqrt[4]{\frac{E_j I_j}{\rho_j A_j}}$ and the a_{jk} coefficients are determined by imposing the boundary conditions (BCs) with $j = 1, 2$ and k ranging from 1 to 4. Enforcing equal transverse displacements and flexural rotations at the ends of the unit cell, where the two beams are coupled with a rigid connection, gives the first set of BCs:

$$y_1(0) = y_2(0) \quad , \quad \theta_1(0) = \theta_2(0) \tag{3a}$$

$$y_1(L) = y_2(L) \quad , \quad \theta_1(L) = \theta_2(L) \tag{3b}$$

with $\theta_j(x) = \frac{dy_j}{dx}$. Since the structure is periodic, the displacements and forces associated with the two boundaries of the unit cell are related by using the Bloch theorem. This yields the second set of BCs:

$$y_1(L) = e^{iqL}y_1(0) \quad , \quad \theta_1(L) = e^{iqL}\theta_1(0) \tag{4a}$$

$$V(L) = e^{iqL}V(0) \quad , \quad M(L) = e^{iqL}M(0) \tag{4b}$$

where q is the wave number and $i = \sqrt{-1}$. Due to the coupling at the boundaries, $M(0) = M_1(0) + M_2(0)$ and $V(0) = V_1(0) + V_2(0)$ where $M_j(x) = E_j I_j \frac{d^2 y_j}{dx^2}$ and $V_j(x) = \frac{dM_j}{dx}$ denote the moment and shear force in each beam.

Substituting the analytical solutions given by (2) into (3) and (4) leads to a system of linear equations for the a_{jk} coefficients, which may be written as

$$[C]\{a\} = 0 \tag{5}$$

with $\{a\} = [a_{11}, a_{12}, a_{13}, a_{14}, a_{21}, a_{22}, a_{23}, a_{24}]^T$. Seeking non-trivial solutions for the above system, by setting the determinant of the coefficient matrix $[C]$ to zero, gives the analytical dispersion relation of the structure, which has a quadratic form in $\cos qL$ (see Appendix A.1 for more details).

Examining the resulting dispersion relation reveals that for arbitrary material and cross-sectional properties of the first beam element- i.e. fixed β_1-, there are only two non-dimensional parameters (namely, $\hat{\rho}\hat{A}$ and $\hat{E}\hat{I}$) that influence the dispersion relation of the system. Here, $\hat{(.)} = \frac{(.)_2}{(.)_1}$. $\hat{\rho}\hat{A}$ indicates the mass ratio between the two beams while $\hat{E}\hat{I}$ shows the stiffness ratio. In Section 3.1, we study how the location and width of the first band gap change when these parameters are varied.

Compliant connections In practice, it may be difficult to have fully-rigid connections. Here, we develop the analytical solution for the case of connections with finite translational and rotational stiffnesses K_s and K_t. The unit cell configuration alongside with the coordinate system in this case is shown in Fig. 1c. The governing equations as well as the general form of solution for $y_j(x)$ $(j = 1, ..., 4)$ are the same as the previous section. However, the boundary conditions are different in this case.

The first set of BCs is determined by imposing continuity of displacements and balance of forces within each beam element:

$$y_1(L/2) = y_2(0) \quad , \quad \theta_1(L/2) = \theta_2(0) \tag{6a}$$

$$y_3(L/2) = y_4(0) \quad , \quad \theta_3(L/2) = \theta_4(0) \tag{6b}$$

$$-V_1(L/2) + V_2(0) + F_s = 0 \tag{6c}$$

$$-V_3(L/2) + V_4(0) - F_s = 0 \tag{6d}$$

$$-M_1(L/2) + M_2(0) + M_s = 0 \tag{6e}$$

$$-M_3(L/2) + M_4(0) - M_s = 0 \tag{6f}$$

In the above, F_s and M_s are the force and moment in the connector springs, respectively and are defined as follows:

$$F_s = K_s[y_2(0) - y_4(0)] \tag{7a}$$
$$M_s = K_t[\theta_2(0) - \theta_4(0)] \tag{7b}$$

The second set of BCs consists of the Bloch boundary conditions:

$$y_2(L/2) = y_1(0)e^{iqL} \quad , \quad \theta_2(L/2) = \theta_1(0)e^{iqL} \tag{8a}$$
$$y_4(L/2) = y_3(0)e^{iqL} \quad , \quad \theta_4(L/2) = \theta_3(0)e^{iqL} \tag{8b}$$
$$V_2(L/2) = V_1(0)e^{iqL} \quad , \quad M_2(L/2) = M_1(0)e^{iqL} \tag{8c}$$
$$V_4(L/2) = V_3(0)e^{iqL} \quad , \quad M_4(L/2) = M_3(0)e^{iqL} \tag{8d}$$

These boundary conditions are used to form a system of linear equations as in the previous section. The dispersion relation is determined by setting the determinant of the coefficient matrix to zero and is proven to be quartic in $\cos qL$ (see Appendix A.2).

2.2 Numerical model

Bloch mode synthesis [39] is used to determine the band structure of the system numerically. We use a standard Finite Element method to construct the mass and stiffness matrices of the unit cell. The matrices are then partitioned according to the interior and interface nodes and the Craig-Bampton method [23] is chosen to represent the normal and constraint modes. Depending on the highest frequency of interest and for the sake of computational efficiency, only a reduced set of the fixed-interface modes (FIM) is kept. Next, Bloch boundary conditions are imposed through interface nodes to create the mass and stiffness matrices of an infinite metamaterial beam. The reduced model is then used for eigenvalue analysis to determine the band structure of the periodic system. Matlab® is used for all numerical simulations in this paper.

3 Results

3.1 Infinite metamaterial beams

Parametric study of the band gap structure in rigidly-connected beams In this section, we study the parametric dependence of the first band gap characteristics in terms of the two independent variables identified in the previous section - i.e. the mass ratio and the stiffness ratio of the two beams.

We consider one of the beams to be a doubly-symmetric I-beam made of concrete with a Young's modulus of 25 GPa and a density of 2400 kg m^{-3}. The dimensions of the flange and web are 150×40 mm and 170×30 mm, respectively. The properties of the other beam are varied to explore the parameter space. The unit cell length, corresponding to the distance between the coupling points, is 1 meter.

Figures 2a and 2b show the variation of the lower and upper edge frequencies with the non-dimensional parameters $\hat{\rho}\hat{A}$ and $\hat{E}\hat{I}$. For a fixed mass ratio, as the stiffness ratio increases, the edge frequencies increase. On the other hand, for a fixed value of stiffness ratio, the lower and upper edge frequencies decrease with an increase in mass ratio. Since for a homogeneous Euler-Bernoulli beam, the phase speed for a wave with radial frequency ω is equal to $\sqrt{\omega}\beta$, the variable $\hat{\beta}$ is, in fact, a measure of the wave's phase speed ratio in the two beams. Fig. 2 suggests that the band gap edge frequencies do not vary significantly in the region close to $\hat{\beta} = 1$, i.e. where the two beams have similar dispersive properties.

Fig. 2c shows the variation of the first band gap width with the non-dimensional parameters $\hat{\rho}\hat{A}$ and $\hat{E}\hat{I}$. When $\hat{\beta}$ is close to 1, the band gap width is very small. When $\hat{\beta}$ is exactly 1, there is no

band gap - even if the two beams have different material and cross-sectional properties. However, as the contrast in the stiffness and mass ratios increases, the band gap width increases as well. In particular, for large stiffness ratios and low mass ratios, the band gap width becomes maximum. A local maximum is also observed in the region with high mass ratios and low stiffness ratios. It should be noted that as the bandwidth increases, so does the frequency corresponding to the lower edge of the band gap. In other words, the set of parameters that maximize bandwidth do not necessarily give the lowest frequency edge. Hence, depending on the target objective, the required mass and stiffness ratio may be tuned.

Fig. 2d shows a contour for the percent ratio between the gap width and the mid-gap frequency as a function of the two non-dimensional variables. At the two ends of the spectrum, the gap width-to-midgap frequency ratio is maximum. Thus, choosing high-contrast properties for the two beams leads to higher normalized band gap widths.

The above discussion suggests that achieving low-frequency band-gaps requires very high mass ratios and very low stiffness ratios; whereas, achieving wide band gaps requires low mass ratios and high stiffness ratios. The two, therefore, lie on the two ends of the spectrum. The high contrast required in β values may be accommodated by a high contrast in material properties of the two beams, a high contrast in cross-sectional properties or a combination of both. The resulting band gaps may be of BS or LR type. In the following section we review a classification of the expected band structure zones and follow with a representative numerical example.

Classification of the band structure zones For rigid connections, the dispersion relation for the coupled beam system is quadratic in $\cos qL$ as shown in Appendix A.1. Therefore, two pairs of wave numbers $\pm q_1$ and $\pm q_2$ are determined for a given frequency Ω. The wave numbers in each pair represent the same characteristic wave but travelling in opposite directions. Therefore, we only consider q_1 and q_2 herein to analyze the band gap structure.

Physically, a flexural wave may be classified as follows based on its corresponding wave number [29, 30]:

(a) Propagating: The wave number is purely real, $q = Re(q)$. In this case, the wave travels over the unit cells without attenuation and only with a phase change.

(b) Attenuating: The real part of the wave number has the form $Re(q) = 0$ or $|Re(q)| = \pi$ and the imaginary part is nonzero. This corresponds to a wave that attenuates while travelling across a unit cell.

(c) Complex: The wave number is complex, i.e. $0 < |Re(q)| < \pi$ and $|Im(q)| > 0$. In this case, the wave is propagating and attenuating as it travels along the structure.

Depending on which category q_1 and q_2 belong to, the system will have four distinct types of dispersion properties at a given frequency Ω:

I. Propagation-Propagation (PP): in this case both waves are propagating without attenuation across the system.

II. Propagation-Attenuation (PA): Only one of the waves propagates through the system and the other gets attenuated as it travels over multiple unit cells.

III. Attenuation-Attenuation (AA): where both wave numbers belong to the attenuation category. In this case, the adjacent cells vibrate either in phase or out of phase, attenuating the waves as they travel through the structure as a result. This behavior is typical of the classical Bragg Scattering phenomenon. Therefore, this region is also called the Bragg Scattering (BS) zone.

IV. Complex (C): The wave numbers q_1 and q_2 belong to category (c) above and are complex-conjugate. In this case, the two wave numbers essentially represent the same characteristic wave that attenuates and experiences a phase change as it travels across a unit cell. This

is usually characteristic of a local resonance mechanism when using a periodic array of resonators. Thus, this region can also be marked as the Local Resonance (LR) zone.

Based on the classification proposed, there are two types of pass bands (PP and PA) and two types of band gaps (AA and C). In the example discussed in the next section, we determine the band structure and study the dispersive behavior of the system based on this classification.

Example To achieve low-frequency band gaps, forming due to a high contrast in β ratios of the two beams, we consider coupling the concrete beam from the previous section to a beam made of a Tungsten alloy (Young's modulus 310 GPa and density 18000 $\mathrm{kg\,m^{-3}}$) with rigid connections. High-density tungsten alloys are widely used for vibration damping in different industries due to their favorable physical properties. This beam element is assumed to have a circular cross section with a radius of 30 millimeters. The length of the unit cell is considered to be 1 meter. The dispersion response of the system is studied in detail next.

The analytical solution given in Appendix A.1 is used to get a comprehensive view of the system's band gap structure (Fig. 3) and unravel the dispersion properties of the periodic system. The regions of interest to us are the AA and C regions, in which both waves get attenuated while traveling across the unit cells either by a BS or LR-type mechanism. The plots show that the first and third band gaps are generated by a blend of BS and LR-type mechanisms. In the first band gap, wave numbers transition from an AA region to a C zone as the frequency increases while for the third band gap, the transition between these zones is reversed. The second band gap, however, forms purely due to BS effects.

It should be noted that the dispersion relation of the waves that propagate freely in the system is governed by the purely real wave numbers while the attenuation properties of the system are dominated by the imaginary part of the wave number that has the lowest absolute value. Having this in mind, the complex band structure in Fig. 3 may be reduced to the simple representation in Fig. 4. Fig. 4a shows the dispersion curves of the periodic system and also serves to demonstrate that the analytical and numerical results match.

Studying the band gap structure of the system shows that the first band gap spans from 199 Hz to 276 Hz with a normalized band gap width of 32.5%. The second band gap edge frequencies are 310 Hz and 524 Hz; this band gap has a normalized gap width of 51.2% . Interestingly, an almost flat dispersion curve lies between the first two band gaps. The ratio of the width of this pass band to the width of the frequency region between 199 Hz and 524 Hz is only 10.4%. Furthermore, waves with frequencies in this pass band region have significantly lower phase velocities than those corresponding to the first and third dispersion lines. These observations indicate that this pass band may be neglected in practice. Doing so, gives a wide band gap with a normalized width of nearly 90%.

Fig. 4b demonstrates the attenuation constants of the system within the band gaps. The figure shows that the first and third band gaps are Fano-shaped and highly asymmetric while the second band gap shows a smooth variation in the attenuation constant. These are well-established properties of the LR and BS band gaps, respectively and have been previously documented in the literature [30, 32, 33, 40].

Effect of connection compliance In this section, we study the effects of connection compliance on the band gap structure and attenuation properties of the system. The unit cell configuration in this case is shown in Fig. 1c. The analytical dispersion relation is determined in a similar manner as before and is found to be quartic in $\cos qL$ (see Appendix A.2). Therefore, four pairs of wave number solutions exist for a given frequency, with each pair representing the same characteristic wave but propagating in opposite directions. The nature of these characteristic waves (whether each is of Attenuating, Propagating or Complex type) determines the band structure of the system.

To facilitate further investigation, we introduce the non-dimensional parameters $\alpha = K_s/(E_1 I_1/L^3)$ and $\gamma = K_t/(E_1 I_1/L)$. Fig. 5 shows the variations in the first band gap properties as α and γ

change. For low values of α, no band gaps exist even at high γ values. This suggests that the coupling between the translational displacements of the two beams is essential for generating band gaps. As α increases, the first band gap starts to form. The plots suggest that the band gap edge frequencies and width increase as the connection stiffness increases. Fig. 5c shows that the variation of the band gap width with the connection stiffness ratios is non-monotonic. Two local regions of maximized band gap width may be identified. The first region occurs for small values of γ ($\ln\gamma < -2$) and a limited range of α values ($2.5 < \ln\alpha < 4.5$). The second region occurs towards the high-stiffness end of the spectrum, where both α and γ are large. Fig. 5d also suggests that the normalized band gap width varies non-monotonically with connection stiffness parameters. The normalized band gap width is maximized in a limited range of parameter values ($2.5 < \ln\alpha < 3.5$, $\ln\gamma < -3.5$).

The analytical solution discussed in Appendix A.2 is used next to study the effect of connection stiffness on the band gap structure and attenuation strength of the system. Two candidate cases are examined: In the first case, γ is set to 0 and in the second case, it is set to 10^3. In both cases, α values of 10,10^2 and 10^3 are considered. Fig. 6 shows how varying the two parameters modifies the dispersion properties of the system. For instance, in the first case, when $\alpha = 10$, there's a possibility of lowering the band gap edge frequency to 98.2 Hz and increasing the normalized gap width to 53.7% in comparison to the case with rigid connections (Fig. 4a). As another example, in the second case ($\gamma = 10^3$), when α is 100, the attenuation strength in the second band gap increases significantly. Whereas, when α is 10 in the same case, the band gap widths are very small, making this set of parameters unfavourable.

It should also be noted that when α and γ are both 10^3, the connection between the two beams may be considered as almost rigid. Thus, the overall band structure for this set of parameters is similar to the one for rigid connections (Fig. 4). Figures 6b and 6d show the effect of connection compliance on the attenuation properties of the periodic structure. The plots indicate that tuning the stiffness of the connection may increase the attenuation strength, change the nature of the attenuation mechanisms and make them interact. The complex band structure of two sample cases are included in Appendix B to highlight the complexity of solution behaviors and the strong interactions between characteristic waves.

Hierarchical systems In this section, we briefly study the effect of coupling more than two beams having different periodicities at different scales on the dispersion properties of the overall structure.

Fig. 7 shows the unit cell configurations and the corresponding dispersion curves for three cases: (i) a concrete and tungsten beam coupled periodically with a unit cell length of 1 meter; (ii) a concrete and tungsten beam coupled periodically with a unit cell length of 0.5 m; and (iii) a concrete and tungsten beam periodically coupled at 0.5 m spacing with the whole pair coupled to a third tungsten beam at 1 m spacing. The third configuration is a combination of the first two and involves two periodicity scales. The figure shows that the interaction between the two periodicity scales in case (iii) has modified the system's band structure, creating band gaps where we previously had propagation zones and affecting the edge frequencies. The effect of hierarchy is more pronounced when comparing cases (ii) and (iii): the edge frequencies of the first band gap are considerably lower in case (iii) and several band gaps form where we had propagation zones in case (ii). The dispersion curves in case (iii) are close to the ones in case (i) for low frequencies but start to deviate from them at higher frequency ranges. For example the fourth band gap in case (iii) forms in a propagation zone of case (i). These findings suggest that this may potentially be an effective intervention technique for changing attenuation properties of existing metamaterial beam structures.

3.2 Finite systems

In order to study the vibration transmittance properties of the system, we calculate the Frequency Response Function (FRF) of two periodically-connected, simply-supported beams with 20 unit

cells. The material and cross-sectional properties of the beams as well as the unit cell length are the same as the example discussed in the previous section. Two cases are considered: one with rigid connections and one with connection stiffness parameters $\alpha = 100$ and $\gamma = 0$. Each beam is divided into 200 finite beam elements. The FRF matrix $[H_{qF}]$ due to a harmonic excitation force of amplitude F_0 can be determined from the FEM model using modal analysis:

$$\begin{aligned} &[M_r]\{\ddot{\eta}_r\} + [C_r]\{\dot{\eta}_r\} + [K_r]\{\eta_r\} = \{F_r\} \\ &[H_{\eta_r f_r}] = [-\Omega^2[M_r] + [K_r] + i\Omega[C_r]]^{-1} \\ &[H_{qF}] = [\Phi][H_{\eta_r f_r}][\Phi^T] \end{aligned} \tag{9}$$

where, $[M_r]$, $[K_r]$ and $[C_r]$ are the modal mass, stiffness and damping matrices respectively. The modal damping coefficient ξ is assumed to be equal for all modes. $\{\eta_r\}$ is the vector of modal coordinates and $F_r = \Phi^T F$ ($F = \{0, 0, F_0 e^{i\Omega t}, 0, ...\}^T$) is the modal forcing vector with $[\Phi]$ being the matrix of eigenvectors.

In all cases, the harmonic excitation is applied at the node adjacent to the left support on the concrete beam and the transverse response is measured at the node adjacent to the right support for each beam. In addition, the node where the harmonic force is applied is not a connection point between the two members. Figures 8a and 9a show the FRF of the transverse displacement for different levels of damping. The grey areas show the band gap regions predicted in the previous section. The figures show that the regions of strong attenuation lie well within the band gaps. The relative strength of attenuation in each region is consistent with the attenuation constants shown in Figures 4b and 6b for the case of rigid and compliant connections, respectively. For example, in the case of the rigid connection, the wave attenuation is intensified in the first and third band gaps, where BS and LR effects blend in and the attenuation constants are larger compared to the second band gap with a BS-type mechanism and smaller attenuation constants. The figure also shows that the FRF peaks corresponding to the resonance frequencies of the structure may be smoothened by a slight increase in the damping coefficient.

Figures 8b and 9b show the Frequency Response Function for different number of unit cells. The figures indicate that as the number of unit cells increases, the reduction in amplitude becomes larger, as is expected in periodic systems.

4 Discussion

We have presented a mathematical model and analytical representation of the dispersion relation for coupled Euler-Bernoulli beams that are periodically joined by rigid or compliant connections. While each homogeneous beam does not individually have band gaps, multiple band gaps emerge when the two beams are connected in parallel. Our results suggest that a high contrast between the phase speeds in the pair of flexural members affects the band structure of the system and its dispersion properties significantly. In particular, we have shown that for high mass ratios and low stiffness ratios, the edge frequencies may be pushed towards low-frequency ranges but only at the cost of band gap width reduction. For low mass and high stiffness ratios, band gaps have remarkably larger widths but form at higher frequencies. Interestingly enough, $\hat{\beta} = 1$, corresponding to the case of two beams having the same phase speed, is the line of symmetry for the normalized gap width. The contour shows an increase in the normalized gap width when moving away from this line.

By analyzing the regions of propagation and attenuation in the band gap structure, we have shown that, just as in the case of discrete periodic resonators, depending on the nature of the wave numbers, two different mechanisms are responsible for band gap formation: Bragg Scattering (BS) and Local Resonance (LR). Constructing a simplified representation of the complex band structure, showed that the attenuation constant varies smoothly in the band gap regions associated with the BS effect while it possesses sharp peaks and is highly asymmetric where LR is the main attenuation mechanism. Thus, unlike the conventional binary configuration, in which heterogeneous flexural components are connected in series, leading to the formation of BS-type band gaps, the proposed

parallel configuration benefits from both BS and LR attenuation mechanisms.

Investigation of the effect of connection compliance shows that the transverse coupling is necessary for band gap formation. Whereas, the elimination of the rotational spring lowers the first band gap edge while increasing its width for a limited range of transverse spring stiffness values. We also showed that tuning the stiffness of the springs may affect the nature of the band gap formation mechanisms as well as the strength of attenuation. Thus, the compliance of the connection may be used as a means of controlling and/or modifying the band structure of the system.

As a preliminary step towards the hierarchical design of metamaterial beam systems, we have demonstrated how adding periodicity in another length scale may affect the dispersion properties of the original structure. The new system has attenuation zones that do not exist in either of the two structures alone. Stacking flexural elements with different unit cell sizes, thus, seems a promising avenue for benefiting from the interaction between the scales and enriching or altering the dispersion properties of a system.

Although a lot of research has been done on periodic and local resonant metamaterials, many have mainly focused on using discrete resonators [27, 41–43] or modelling the effect of continuous resonators, such as beams, with spring-mass assemblies [28]. Considering that these discrete resonators affect the dispersion properties of the main system by creating band gaps in regions close to their natural frequency, the use of continuous elements with a countable infinity set of natural frequencies seems to offer more possibilities for enriching the system's band structure. Our study, in particular, shows that by periodically connecting two Euler-Bernoulli beams, a new system with several LR and BS band gaps is created and that varying the coupling strength, by changing the connection's compliance, will let the two mechanisms interact.

As pointed out briefly in Section 1, unconventional designs have been recently proposed that offer a broader range of dispersion characteristics [44]. Among these novel configurations are the concepts of resonator-to-resonator interactions [17, 18] and nonlocal resonances [19]. For example, in Beli et al. 2018 [18], the interaction between the transverse and rotational modes of a resonator chain consisting of beam elements has been used to achieve a wider band gap in comparison to the case where the resonators perform independently. The authors show how certain Bloch wave modes of the system correspond to the resonance frequencies of the resonator chain. DePauw et al. 2018 [19] propose a configuration called a Phononic Resonator in which each resonator can directly interact with the neighboring masses in the main chain. It is then shown how tuning the stiffness and mass ratios of the main and resonator masses can change the nature of the attenuation mechanism leading to the system behaving as a Phononic Crystal or an Acoustic Metamaterial. In the present work, there can be no distinction between the host and resonating elements since the members periodically connected are both continuous. Therefore, we conjecture that, unlike the previous studies, the resonance frequencies at which the attenuation peaks occur do not solely depend on the properties of one element or the other. Furthermore, Apart from the fact that tuning the physical parameters of the problem could change the nature of the attenuation mechanism within band gaps (such as that observed in DePauw et al. 2018), a mixture of BS and LR effects is observed within certain band gaps. Similar phenomenon has been reported in [29, 31, 33].

Future extensions of this work may include further investigation of the hierarchical coupling, which significantly increases the dimension of the parameter space. Given the surge of interest in non-reciprocal wave propagation, it may be of interest to explore the influence of space-time modulation of the coupled beams' elastic properties or the time modulation of the connection compliance on the overall dispersion relation structure and directional control of the energy flow. Furthermore, combination of coupled beams and discrete resonators may be considered as this setup may enable further tuning of the band gap structure as well as the formation of band gaps in lower frequencies. Another intriguing route for future investigations is controlling the transitions between different propagation/attenuation zones in the band structure by tuning the design parameters. The coefficients of the dispersion relation, presented in Appendix A.1, may be used to describe the different propagation characteristics of the system with rigid connections on the invariant's plane $J_1 - J_2$ [45]. A mapping from the invariant plane to the physical parameter plane could then be used to visualize the transition between propagation domains as the parameters are varied. A similar study could be carried out for general systems with dispersion relations that are of fourth order in

$\cos qL$.

5 Conclusions

In this work, We investigated the dynamics and dispersion properties of flexural elements that are periodically coupled in parallel using rigid or compliant connections. our main conclusions are summarized as follows:

- For rigid connections between the two elements, a high contrast between the phase speeds affects the band structure of the system significantly. In particular, for the first band gap, high (low) mass ratios and low (high) stiffness ratios result in lower (higher) edge frequencies and narrower (wider) band gaps.
- Unlike the conventional configuration, in which beam elements of different material/geometric properties are connected in series, leading to BS-type band gaps, the proposed configuration benefits from both BS and LR mechanisms.
- The connection compliance may be used to modify the system's band structure by opening/closing gaps. Tuning the stiffness parameters may lower some band gap edge frequencies, increase their width, intensify the attenuation strength or change the nature of the attenuation mechanisms.
- Stacking flexural elements at different periodicity lengths may modify the band structure by closing/opening band gaps.

6 Acknowledgements

The authors are grateful to Katie Matlack and Alexander Vakakis for the intriguing discussions. This research has been supported by funds from Campus Research Board of University of Illinois Urbana Champaign (RB17043), and the National Science Foundation grants (CMMI-Award Number 1435920) and (CAREER Award Number 1753249).

7 Figures

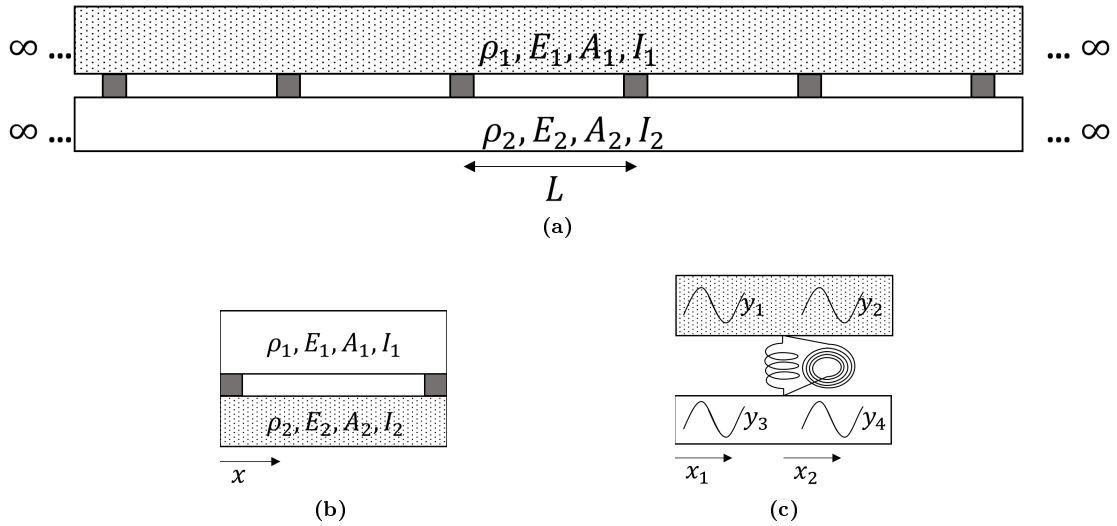

Fig. 1. Model setup. (a) Metamaterial beam structure consisting of two uniform beams that are periodically attached. (b) Unit cell configuration for rigid connections. (c) Unit cell configuration for compliant connections.

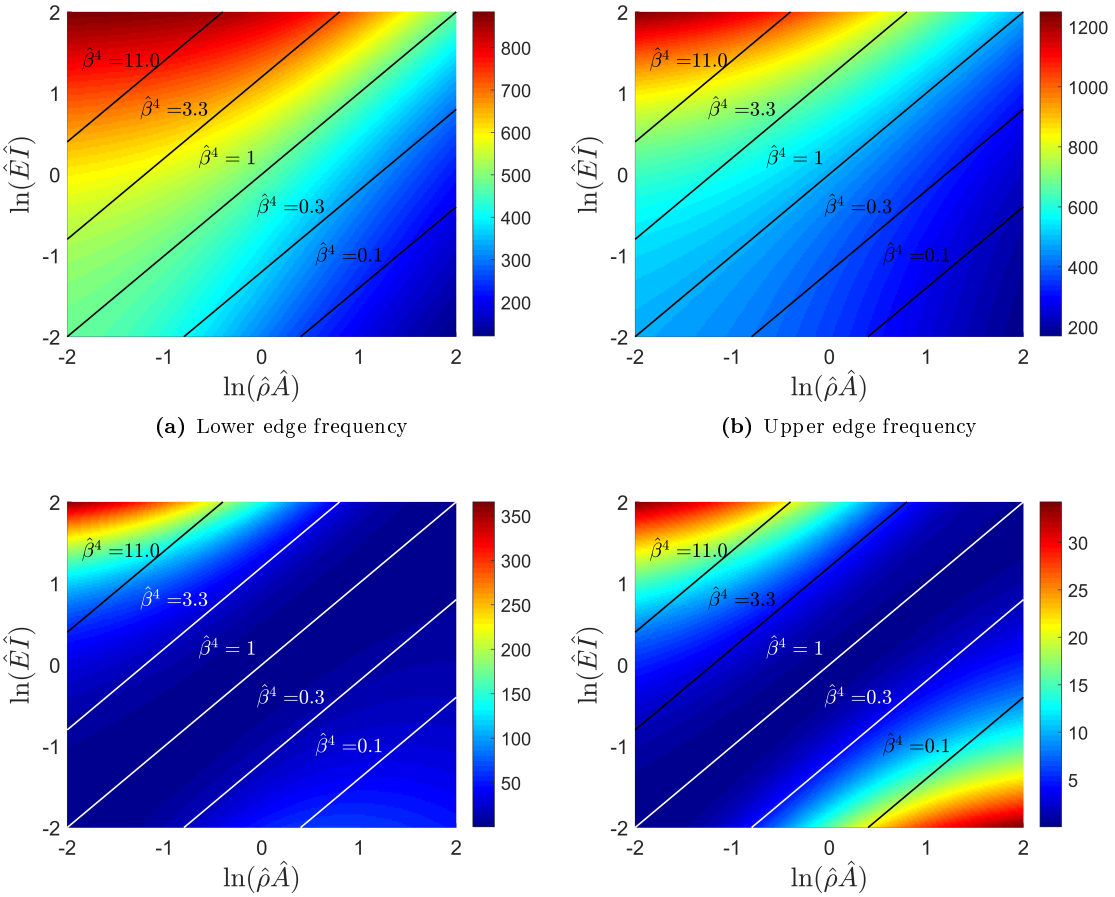

(a) Lower edge frequency

(b) Upper edge frequency

(c) Band gap width

(d) Normalized gap width(%)

Fig. 2. Variations of the first band gap properties with changes in mass ratio ($\hat{\rho}\hat{A}$) and stiffness ratio ($\hat{E}\hat{I}$). $\hat{\beta}$ represents the ratio of the wave phase speed for the two beams. Lines of constant $\hat{\beta}$ give another measure for comparing the variations of the properties. (a)-(b) The band gap forms at lower frequencies as the mass ratio (stiffness ratio) increases (decreases). (c) The band gap width increases for high stiffness ratios along with low mass ratios. (d) The normalized gap width increases as we move to the two ends of the spectrum. (For the interpretation of the color references in this figure, the reader is referred to the web version of the article.)

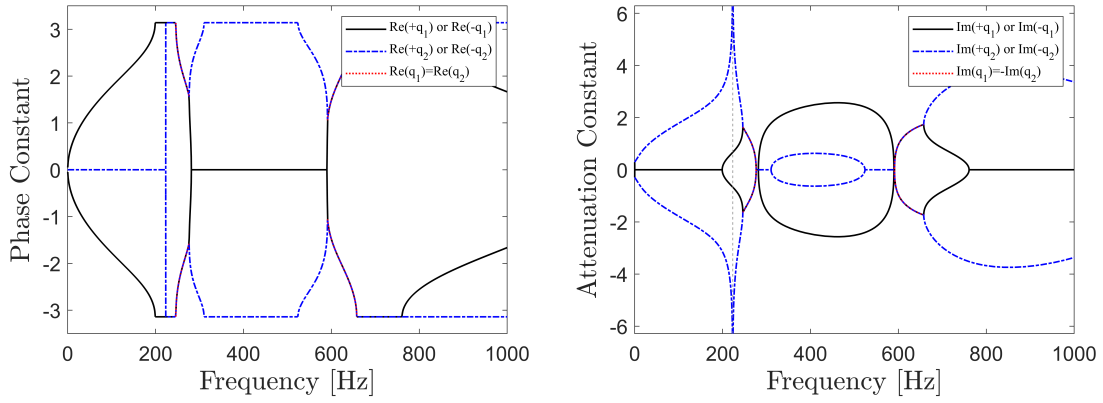

(a) (b)

Fig. 3. The complex band structure of the periodic flexural system: (a) shows the real part of the wave number pair, which determines the dispersion relation of propagating waves and (b) shows the imaginary part of the wave number pair, governing the attenuation properties of the system.

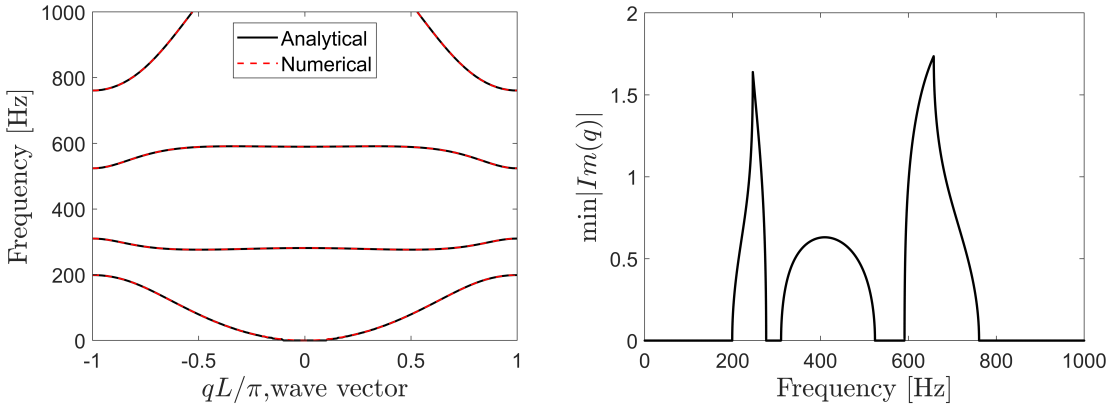

(a) (b)

Fig. 4. A simplified representation of the complex band structure shown in Figure 3. (a) Dispersion curves of the periodically-coupled concrete and Tungsten beams. (b) Minimum absolute value of attenuation constants.

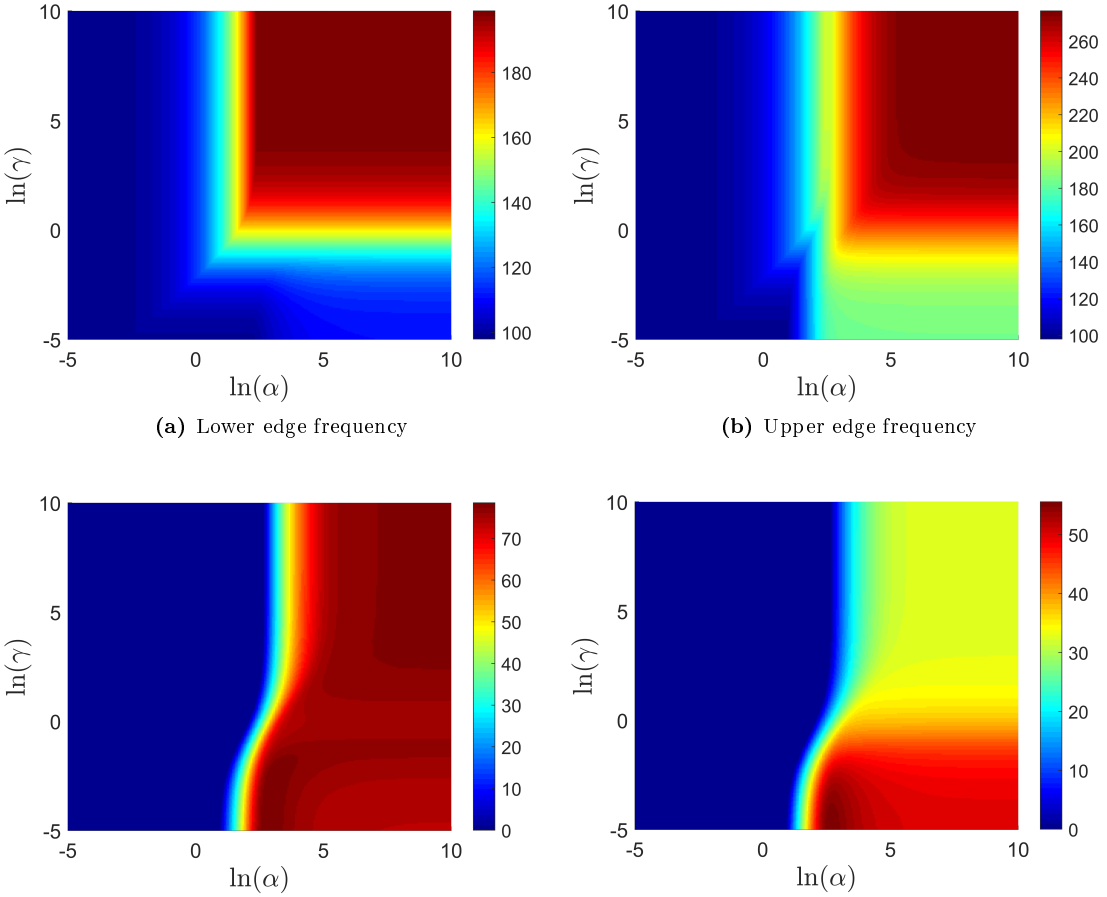

(a) Lower edge frequency

(b) Upper edge frequency

(c) Band gap width

(d) Normalized gap width(%)

Fig. 5. Variations of the first band gap properties with changes in the normalized stiffnesses of the translational and rotational springs (α and γ). (a)-(b) The edge frequencies increase as the stiffness of the connection increases. (c) The band gap width reaches its maximum in two regions: the stiff end of the spectrum (high α and γ values) and a limited region for very small γ values. (d) The maximum normalized gap width occurs in a localized region of α values for very low rotational stiffnesses. (For the interpretation of the color references in this figure, the reader is referred to the web version of the article.)

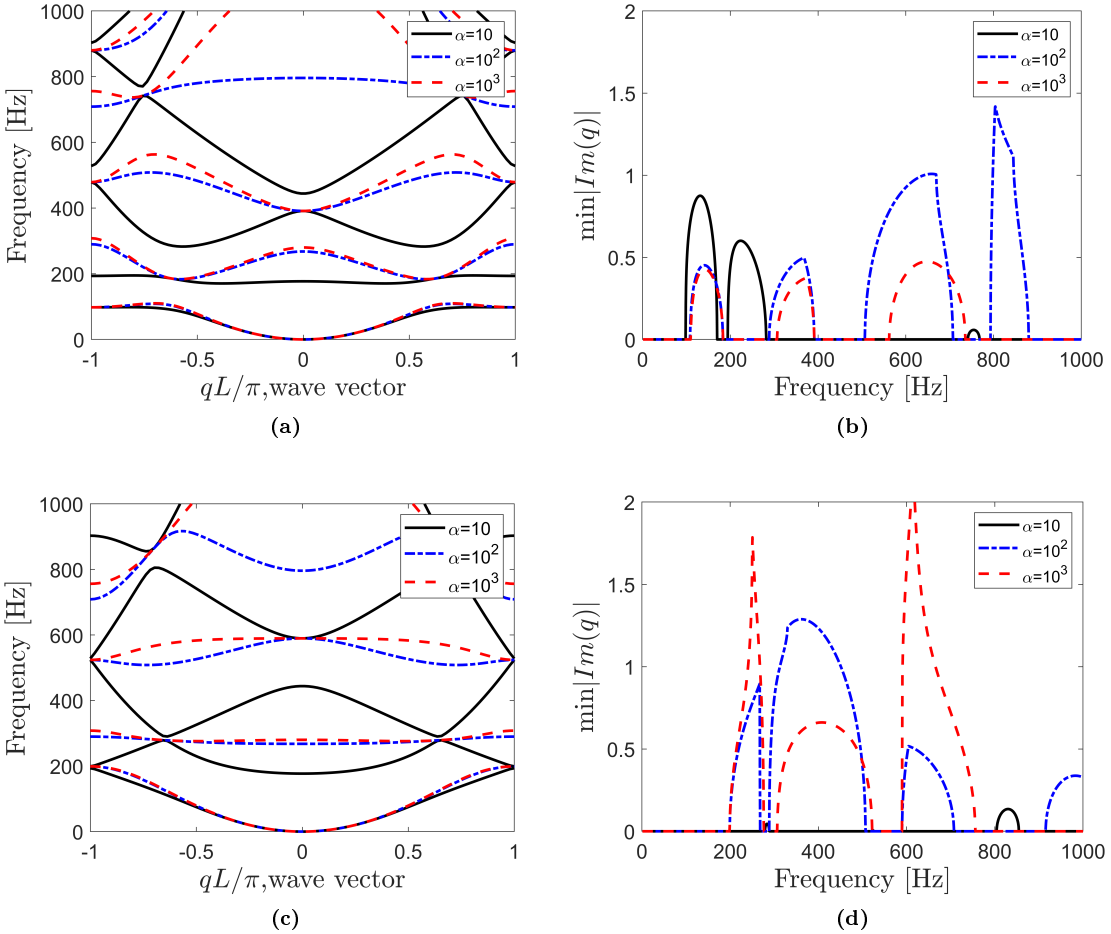

Fig. 6. Effect of connection compliance on the band structure and attenuation strength of the system. (a)-(b): $\gamma = 0$. (c)-(d): $\gamma = 10^3$

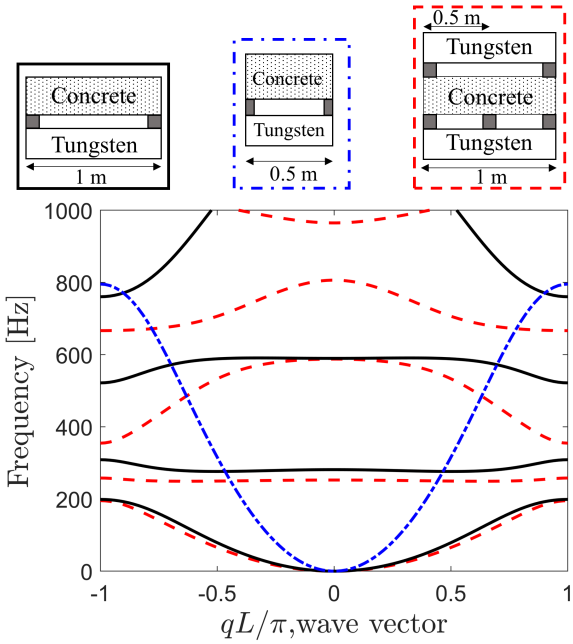

Fig. 7. The dispersion plots corresponding to the three unit cell configurations in the insert: cases (i)-(iii) as described in the text plotted with solid black line, blue dashed-dotted line and red dashed line, respectively.

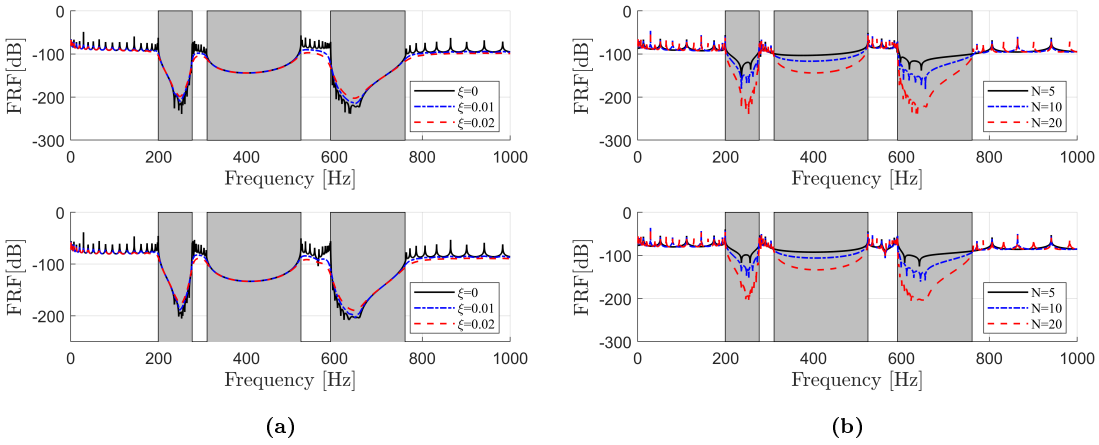

(a) **(b)**

Fig. 8. Steady-state response of the periodic system: (a) Frequency Response Function of the concrete beam (above) and Tungsten beam (below) for a structure with 20 unit cells and different damping coefficients. (b) Comparison of the undamped Frequency Response Functions of the concrete beam (above) and Tungsten beam (below) for structures with different number of unit cells.

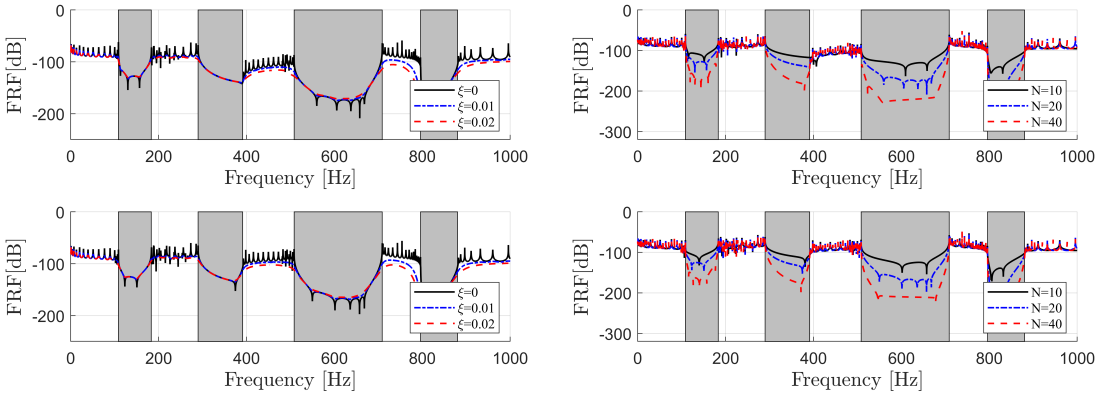

Fig. 9. Steady-state response of the periodic system with compliant connections ($\gamma = 0$, $\alpha = 100$): (a) Frequency Response Function of the concrete beam (above) and Tungsten beam (below) for a structure with 20 unit cells and different damping coefficients. (b) Comparison of the undamped Frequency Response Functions of the concrete beam (above) and Tungsten beam (below) for structures with different number of unit cells.

Appendix A Analytical formulation of the dispersion relation for coupled beams in a parallel configuration

A.1 Rigid connections

We introduce the variables $k_b^{(1)} = \frac{\sqrt{\omega}}{\beta_1}$ and $k_b^{(2)} = \frac{\sqrt{\omega}}{\beta_2}$ and use the propagation constant, $\mu = iqL$, for convenience. Substituting (2) in (3) and (4), we can construct a system of linear equations as follows

$$[C]\{a\} = 0 \tag{A.1}$$

Matrix $[C]$ is a function of material properties and the geometry of the two beam sections as well as the frequency ω and wave number q. In order for the system to have nontrivial solutions, the determinant of this matrix must be set to zero. Doing so and rearranging parameters gives the dispersion relation in the following form

$$(e^{2\mu} + e^{-2\mu}) + J_1(e^{\mu} + e^{-\mu}) + J_2 = 0 \tag{A.2}$$

or

$$\cosh^2\mu + \frac{J_1}{2}\cosh\mu + \frac{J_2 - 2}{4} = 0 \tag{A.3}$$

where, $J_1 = \frac{H_1}{H_3}$ and $J_2 = \frac{H_2}{H_3}$ and

$$H_1 = 2\Big[\sum_{i=1}^{2} E^{(i)}I^{(i)}\lambda^{(i)} \sum_{i=1}^{2} E^{(i)}I^{(i)}\bar{\delta}^{(i)} - \sum_{i=1}^{2} E^{(i)}I^{(i)}\bar{\lambda}^{(i)} \sum_{i=1}^{2} E^{(i)}I^{(i)}\delta^{(i)}\Big] \tag{A.4a}$$

$$H_2 = 4\Big[-\big(\sum_{i=1}^{2} E^{(i)}I^{(i)}\eta^{(i)}\big)^2 + \sum_{i=1}^{2} E^{(i)}I^{(i)}\lambda^{(i)} \sum_{i=1}^{2} E^{(i)}I^{(i)}\delta^{(i)}\Big] \tag{A.4b}$$

$$H_3 = \big(\sum_{i=1}^{2} E^{(i)}I^{(i)}\eta^{(i)}\big)^2 - \sum_{i=1}^{2} E^{(i)}I^{(i)}\bar{\lambda}^{(i)} \sum_{i=1}^{2} E^{(i)}I^{(i)}\bar{\delta}^{(i)} \tag{A.4c}$$

The superscript i indicates element number. The parameters $\lambda^{(i)}$, $\delta^{(i)}$, $\bar{\lambda}^{(i)}$, $\bar{\delta}^{(i)}$ and $\eta^{(i)}$ $(i = 1, 2)$ are defined as follows

$$\lambda^{(i)} = [\cos(k_b^{(i)}L)\sinh(k_b^{(i)}L) + \sin(k_b^{(i)}L)\cosh(k_b^{(i)}L)](k_b^{(i)}L)^3/\Delta^{(i)} \tag{A.5a}$$

$$\delta^{(i)} = [-\cos(k_b^{(i)}L)\sinh(k_b^{(i)}L) + \sin(k_b^{(i)}L)\cosh(k_b^{(i)}L)](k_b^{(i)}L)/\Delta^{(i)} \tag{A.5b}$$

$$\eta^{(i)} = [-\cos(k_b^{(i)}L) + \cosh(k_b^{(i)}L)](k_b^{(i)}L)^2/\Delta^{(i)} \tag{A.5c}$$

$$\bar{\lambda}^{(i)} = [\sin(k_b^{(i)}L) + \sinh(k_b^{(i)}L)]/(k_b^{(i)}L)^3\Delta^{(i)} \tag{A.5d}$$

$$\bar{\delta}^{(i)} = [-\sin(k_b^{(i)}L) + \sinh(k_b^{(i)}L)](k_b^{(i)}L)/\Delta^{(i)} \tag{A.5e}$$

$$\Delta^{(i)} = 1 - \cos(k_b^{(i)}L)\cosh(k_b^{(i)}L) \tag{A.5f}$$

Examining the parameters involved reveals that for a fixed unit-cell length and chosen material and cross-sectional properties of the first beam element, there are only two non-dimensional parameters (namely, $\hat{\rho}\hat{A}$ and $\hat{E}\hat{I}$) that influence the dispersion relation of the system.

A.2 Compliant connections

The problem is formulated as in the previous case. The general solutions can be written in a similar form for all four beam elements (Fig. 1c), yielding sixteen unknown coefficients. Setting the determinant of the matrix of coefficients to zero gives the dispersion relation in the following form

$$(e^{4\mu} + e^{-4\mu}) + J_1^*(e^{3\mu} + e^{-3\mu}) + J_2^*(e^{2\mu} + e^{-2\mu}) + J_3^*(e^{\mu} + e^{-\mu}) + J_4^* = 0 \tag{A.6}$$

or

$$\cosh^4\mu + \frac{J_1^*}{2}\cosh^3\mu + \frac{J_2^* - 4}{4}\cosh^2\mu + \frac{J_3^* - 3J_1^*}{8}\cosh\mu + \frac{J_4^* - J_2^* + 1}{8} = 0 \tag{A.7}$$

Again, the coefficients of this fourth-order equation are functions of the material and cross-sectional properties and stiffness parameters α and γ. The mathematical expressions of these coefficients will not be presented here.

Appendix B Complex band structure for compliant connections

Here, we present the complex band structure of the system with compliant connections for two sample cases: one corresponds to $\alpha = 100$ and $\gamma = 0$ while the other corresponds to $\alpha = 1000$ and $\gamma = 0$. Figures B.1a and B.1b show that within the second band gap, all wave number solutions are of Attenuating type; however, the solution behavior changes within the third band gap. This band gap starts with two Complex and two Attenuating wave number pairs but all solutions become Attenuating as the frequency increases. Figures B.1c and B.1d suggest that within the second band gap, all wave numbers are Attenuating while the third one forms with a complex-conjugate pair and two attenuating ones. The solution behavior doesn't change within the band gap in this case. The plots highlight the complexity of the band structure and the strong interactions between the characteristic waves when the connections are not rigid. The observations encourage further future investigation to characterize the propagation/attenuation zones corresponding to different solution behaviors.

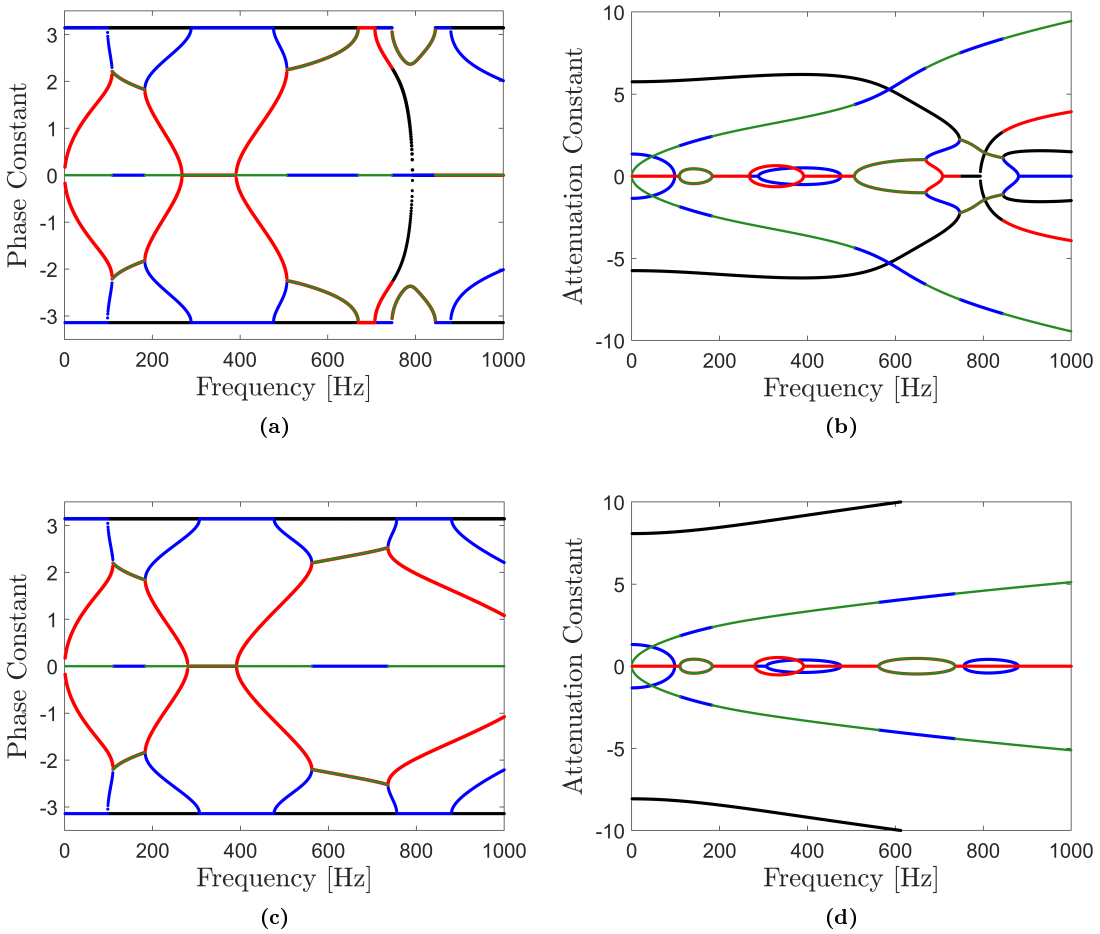

Fig. B.1. The complex band structure of the periodic flexural system with compliant connections for $\gamma = 0$, $\alpha = 100$ (above) and $\alpha = 1000$ (below). The different colors show the four characteristic wave solutions. (a) and (c) show the real part of the wave numbers, which determines the dispersion relation of propagating waves. (b) and (d) show the imaginary part of the wave numbers, governing the attenuation properties of the system. (Colored version of this figure is available online).

References

[1] Dianlong Yu et al. "Vibration reduction by using the idea of phononic crystals in a pipe-conveying fluid". In: *Journal of Sound and Vibration* (2008). ISSN: 0022460X. DOI: 10.1016/j.jsv.2008.04.009.

[2] M. Brun et al. "Asymptotics of eigenfrequencies in the dynamic response of elongated multi-structures". In: *Proceedings of the Royal Society A: Mathematical, Physical and Engineering Sciences* 468.2138 (2012), pp. 378–394. ISSN: 14712946. DOI: 10.1098/rspa.2011.0415.

[3] Michele Brun, Alexander B. Movchan, and Ian S. Jones. "Phononic Band Gap Systems in Structural Mechanics: Finite Slender Elastic Structures and Infinite Periodic Waveguides". In: *Journal of Vibration and Acoustics* (2013). ISSN: 0739-3717. DOI: 10.1115/1.4023819.

[4] G. Carta, G. F. Giaccu, and M. Brun. "A phononic band gap model for long bridges. The 'Brabau' bridge case". In: *Engineering Structures* (2017). ISSN: 18737323. DOI: 10.1016/j.engstruct.2017.01.064.

[5] K S Novoselov et al. "Electric field effect in atomically thin carbon films." In: *Science (New York, N.Y.)* 306.5696 (Oct. 2004), pp. 666–9. ISSN: 1095-9203. DOI: 10.1126/science.1102896. URL: http://www.ncbi.nlm.nih.gov/pubmed/15499015.

[6] Mahmoud I. Hussein, Michael J. Leamy, and Massimo Ruzzene. "Dynamics of Phononic Materials and Structures: Historical Origins, Recent Progress, and Future Outlook". In: *Applied Mechanics Reviews* (2014). ISSN: 0003-6900. DOI: 10.1115/1.4026911.

[7] S. Krödel, N. Thomé, and C. Daraio. "Wide band-gap seismic metastructures". In: *Extreme Mechanics Letters* 4 (Sept. 2015), pp. 111–117. ISSN: 2352-4316. DOI: 10.1016/J.EML.2015.05.004. URL: https://www.sciencedirect.com/science/article/pii/S2352431615000772.

[8] D.J. Colquitt et al. "Seismic metasurfaces: Sub-wavelength resonators and Rayleigh wave interaction". In: *Journal of the Mechanics and Physics of Solids* 99 (Feb. 2017), pp. 379–393. ISSN: 0022-5096. DOI: 10.1016/J.JMPS.2016.12.004. URL: https://www.sciencedirect.com/science/article/pii/S002250961630549X.

[9] Antonio Palermo et al. "Large scale metasurfaces for seismic waves control". In: *The Journal of the Acoustical Society of America* 143.3 (Mar. 2018), pp. 1713–1713. ISSN: 0001-4966. DOI: 10.1121/1.5035578. URL: http://asa.scitation.org/doi/10.1121/1.5035578.

[10] Filippo Casadei et al. "Piezoelectric resonator arrays for tunable acoustic waveguides and metamaterials". In: *Journal of Applied Physics* 112.6 (Sept. 2012), p. 064902. ISSN: 0021-8979. DOI: 10.1063/1.4752468. URL: http://aip.scitation.org/doi/10.1063/1.4752468.

[11] Raj Kumar Pal and Massimo Ruzzene. "Edge waves in plates with resonators: an elastic analogue of the quantum valley Hall effect". In: *New Journal of Physics* 19.2 (Feb. 2017), p. 025001. ISSN: 1367-2630. DOI: 10.1088/1367-2630/aa56a2. URL: http://stacks.iop.org/1367-2630/19/i=2/a=025001?key=crossref.80ac1277a42295ce70d69c8279634782.

[12] Amir Darabi et al. "Broadband Bending of Flexural Waves: Acoustic Shapes and Patterns". In: *Scientific Reports* 8.1 (Dec. 2018), p. 11219. ISSN: 2045-2322. DOI: 10.1038/s41598-018-29192-1. URL: http://www.nature.com/articles/s41598-018-29192-1.

[13] Shu Zhang, Chunguang Xia, and Nicholas Fang. "Broadband Acoustic Cloak for Ultrasound Waves". In: *Physical Review Letters* 106.2 (Jan. 2011), p. 024301. ISSN: 0031-9007. DOI: 10.1103/PhysRevLett.106.024301. URL: https://link.aps.org/doi/10.1103/PhysRevLett.106.024301.

[14] Ahmad Zareei and Mohammad-Reza Alam. "Broadband cloaking of flexural waves". In: *Physical Review E* 95.6 (June 2017), p. 063002. ISSN: 2470-0045. DOI: 10.1103/PhysRevE.95.063002. URL: http://link.aps.org/doi/10.1103/PhysRevE.95.063002.

[15] Guancong Ma and Ping Sheng. "Acoustic metamaterials: From local resonances to broad horizons". In: *Science Advances* 2.2 (Feb. 2016), e1501595. ISSN: 2375-2548. DOI: 10.1126/sciadv.1501595. URL: http://advances.sciencemag.org/lookup/doi/10.1126/sciadv.1501595.

[16] Zhengyou Liu et al. "Locally resonant sonic materials". In: *Science (New York, N.Y.)* 289.5485 (Sept. 2000), pp. 1734–6. ISSN: 1095-9203. DOI: 10.1126/SCIENCE.289.5485.1734. URL: http://www.ncbi.nlm.nih.gov/pubmed/10976063.

[17] Guobiao Hu et al. "Acoustic metamaterials with coupled local resonators for broadband vibration suppression". In: *AIP Advances* 7.2 (Feb. 2017), p. 025211. ISSN: 2158-3226. DOI: 10.1063/1.4977559. URL: http://aip.scitation.org/doi/10.1063/1.4977559.

[18] D. Beli, J.R.F. Arruda, and M. Ruzzene. "Wave propagation in elastic metamaterial beams and plates with interconnected resonators". In: *International Journal of Solids and Structures* 139-140 (May 2018), pp. 105–120. ISSN: 0020-7683. DOI: 10.1016/J.IJSOLSTR.2018.01.027. URL: https://www.sciencedirect.com/science/article/pii/S0020768318300295.

[19] D. DePauw, H. Al Ba'ba'a, and M. Nouh. "Metadamping and energy dissipation enhancement via hybrid phononic resonators". In: *Extreme Mechanics Letters* 18 (Jan. 2018), pp. 36–44. ISSN: 2352-4316. DOI: 10.1016/J.EML.2017.11.002. URL: https://www.sciencedirect.com/science/article/pii/S2352431617301451.

[20] J.W. Miles. "Vibrations of Beams on Many Supports". In: *Proceedings of the American Society of Civil Engineers* 82.1 (1956), pp. 1–9.

[21] Eric E. Ungar. "Steady-State Responses of One-Dimensional Periodic Flexural Systems". In: *The Journal of the Acoustical Society of America* 39.March 1965 (1965). ISSN: NA. DOI: 10.1121/1.1909967.

[22] Hong Jun Xiang and Zhi Fei Shi. "Analysis of flexural vibration band gaps in periodic beams using differential quadrature method". In: *Computers and Structures* (2009). ISSN: 00457949. DOI: 10.1016/j.compstruc.2009.07.009.

[23] Changwei Zhou et al. "Application of wave finite element method on reduced models for the analysis of flexural waves in periodic beams". In: *1st Euro Mediterranean Conference on Structural Dynamics and Vibroacoustics*. Apr. 2013. URL: https://hal.archives-ouvertes.fr/hal-01054911/.

[24] D. J. Thompson. "A continuous damped vibration absorber to reduce broad-band wave propagation in beams". In: *Journal of Sound and Vibration* (2008). ISSN: 10958568. DOI: 10.1016/j.jsv.2007.09.038.

[25] Yong Xiao, Jihong Wen, and Xisen Wen. "Broadband locally resonant beams containing multiple periodic arrays of attached resonators". In: *Physics Letters, Section A: General, Atomic and Solid State Physics* 376.16 (2012), pp. 1384–1390. ISSN: 03759601. DOI: 10.1016/j.physleta.2012.02.059. URL: http://dx.doi.org/10.1016/j.physleta.2012.02.059.

[26] Vagner Candido de Sousa et al. "Adaptive locally resonant metamaterials leveraging shape memory alloys". In: *Journal of Applied Physics* 124.6 (Aug. 2018), p. 064505. ISSN: 0021-8979. DOI: 10.1063/1.5031168. URL: http://aip.scitation.org/doi/10.1063/1.5031168.

[27] Christopher Sugino et al. "On the mechanism of bandgap formation in locally resonant finite elastic metamaterials". In: *Journal of Applied Physics* 120.13 (Oct. 2016), p. 134501. ISSN: 0021-8979. DOI: 10.1063/1.4963648. URL: http://aip.scitation.org/doi/10.1063/1.4963648.

[28] Hongwei Sun, Xingwen Du, and P. Frank Pai. "Theory of metamaterial beams for broadband vibration absorption". In: *Journal of Intelligent Material Systems and Structures* (2010). ISSN: 1045389X. DOI: 10.1177/1045389X10375637.

[29] Michael Yu Wang and Xiaoming Wang. "Frequency band structure of locally resonant periodic flexural beams suspended with force–moment resonators". In: *Journal of Physics D: Applied Physics* 46.25 (June 2013), p. 255502. ISSN: 0022-3727. DOI: 10.1088/0022-3727/46/25/255502. URL: http://stacks.iop.org/0022-3727/46/i=25/a=255502?key=crossref.9b473123b46bd1d39f00f9c4a4260172.

[30] Yong Xiao et al. "Theoretical and Experimental Study of Locally Resonant and Bragg Band Gaps in Flexural Beams Carrying Periodic Arrays of Beam-Like Resonators". In: *Journal of Vibration and Acoustics* 135.4 (June 2013), p. 041006. ISSN: 0739-3717. DOI: 10.1115/1.4024214. URL: http://vibrationacoustics.asmedigitalcollection.asme.org/article.aspx?doi=10.1115/1.4024214.

[31] Yong Xiao et al. "Flexural wave propagation in beams with periodically attached vibration absorbers: Band-gap behavior and band formation mechanisms". In: *Journal of Sound and Vibration* (2013). ISSN: 0022460X. DOI: 10.1016/j.jsv.2012.09.035.

[32] Liao Liu and Mahmoud I. Hussein. "Wave Motion in Periodic Flexural Beams and Characterization of the Transition Between Bragg Scattering and Local Resonance". In: *Journal of Applied Mechanics* 79.1 (Jan. 2012), p. 011003. ISSN: 00218936. DOI: 10.1115/1.4004592. URL: http://appliedmechanics.asmedigitalcollection.asme.org/article.aspx?articleid=1421388.

[33] Xiaoming Wang and Michael Yu Wang. "An analysis of flexural wave band gaps of locally resonant beams with continuum beam resonators". In: *Meccanica* 51.1 (Jan. 2016), pp. 171–178. ISSN: 0025-6455. DOI: 10.1007/s11012-015-0197-x. URL: http://link.springer.com/10.1007/s11012-015-0197-x.

[34] G.S. Gupta. "Dynamics of Periodically Stiffened Structures Using a Wave Approach". PhD thesis. University of Southampton (United Kingdom), 1971. URL: https://search-proquest-com.proxy2.library.illinois.edu/docview/301336247?accountid=14553.

[35] Rong Chen and Tianxing Wu. "Dynamic characteristics of a periodic rib-skin structure". In: *Journal of Vibration and Control* 22.3 (Feb. 2016), pp. 662–677. ISSN: 1077-5463. DOI: 10.1177/1077546314531808. URL: http://journals.sagepub.com/doi/10.1177/1077546314531808.

[36] Junfang Wang, Cheuk Ming Mak, and Yi Yun. "A methodology for direct identification of characteristic wave-types in a finite periodic dual-layer structure with transverse connection". In: *Journal of Vibration and Control* 18.9 (Aug. 2012), pp. 1406–1414. ISSN: 1077-5463. DOI: 10.1177/1077546311419699. URL: http://journals.sagepub.com/doi/10.1177/1077546311419699.

[37] Huang Xiuchang et al. "Design and optimization of periodic structure mechanical filter in suppression of foundation resonances". In: *Journal of Sound and Vibration* 330.20 (Sept. 2011), pp. 4689–4712. ISSN: 0022-460X. DOI: 10.1016/J.JSV.2011.05.027. URL: https://www.sciencedirect.com/science/article/pii/S0022460X11004123%7B%5C#%7Df0020.

[38] Qianli Chen and Ahmed Elbanna. "Emergent wave phenomena in coupled elastic bars: From extreme attenuation to realization of elastodynamic switches". In: *Scientific Reports* (2017). ISSN: 20452322. DOI: 10.1038/s41598-017-16364-8.

[39] Dimitri Krattiger and Mahmoud I. Hussein. "Bloch mode synthesis: Ultrafast methodology for elastic band-structure calculations". In: *Physical Review E - Statistical, Nonlinear, and Soft Matter Physics* (2014). ISSN: 15502376. DOI: 10.1103/PhysRevE.90.063306.

[40] C. Goffaux et al. "Evidence of Fano-Like Interference Phenomena in Locally Resonant Materials". In: *Physical Review Letters* 88.22 (May 2002), p. 225502. ISSN: 0031-9007. DOI: 10.1103/PhysRevLett.88.225502. URL: https://link.aps.org/doi/10.1103/PhysRevLett.88.225502.

[41] P. Frank Pai. "Metamaterial-based Broadband Elastic Wave Absorber". In: *Journal of Intelligent Material Systems and Structures* 21.5 (Mar. 2010), pp. 517–528. ISSN: 1045-389X. DOI: 10.1177/1045389X09359436. URL: http://journals.sagepub.com/doi/10.1177/1045389X09359436.

[42] P. Frank Pai, Hao Peng, and Shuyi Jiang. "Acoustic metamaterial beams based on multi-frequency vibration absorbers". In: *International Journal of Mechanical Sciences* 79 (Feb. 2014), pp. 195–205. ISSN: 0020-7403. DOI: 10.1016/J.IJMECSCI.2013.12.013. URL: https://www.sciencedirect.com/science/article/pii/S0020740313003482.

[43] Yong Xiao et al. "Formation and coupling of band gaps in a locally resonant elastic system comprising a string with attached resonators". In: *Physics Letters A* 375.12 (Mar. 2011), pp. 1485–1491. ISSN: 0375-9601. DOI: 10.1016/J.PHYSLETA.2011.02.044. URL: https://www.sciencedirect.com/science/article/pii/S0375960111002428.

[44] Clémence L. Bacquet et al. "Metadamping: Dissipation Emergence in Elastic Metamaterials". In: *Advances in Applied Mechanics* 51 (Jan. 2018), pp. 115–164. ISSN: 0065-2156. DOI: 10.1016/BS.AAMS.2018.09.001. URL: https://www.sciencedirect.com/science/article/pii/S0065215618300024.

[45] F. ROMEO and A. LUONGO. "INVARIANT REPRESENTATION OF PROPAGATION PROPERTIES FOR BI-COUPLED PERIODIC STRUCTURES". In: *Journal of Sound and Vibration* 257.5 (Nov. 2002), pp. 869–886. ISSN: 0022-460X. DOI: 10.1006/JSVI.2002.5065. URL: https://www.sciencedirect.com/science/article/pii/S0022460X02950650.